Tomographic phase microscopy of living three-dimensional cell cultures

Arkadiusz Kuś
Michał Dudek
Björn Kemper
Małgorzata Kujawińska
Angelika Vollmer

Tomographic phase microscopy of living three-dimensional cell cultures

Arkadiusz Kuś,[a,]* Michał Dudek,[a] Björn Kemper,[b,c] Małgorzata Kujawińska,[a] and Angelika Vollmer[b]
[a]Warsaw University of Technology, Institute of Micromechanics and Photonics, Photonics Engineering Division, Faculty of Mechatronics, Św. A. Boboli 8 Street, 02-525 Warsaw, Poland
[b]University of Münster, Center for Biomedical Optics and Photonics, Robert-Koch-Strasse 45, 48149 Münster, Germany
[c]University of Münster, Biomedical Technology Center of the Medical Faculty, Mendelstraße 17 17, 48149 Münster, Germany

Abstract. A successful application of self-interference digital holographic microscopy in combination with a sample-rotation-based tomography module for three-dimensional (3-D) label-free quantitative live cell imaging with subcellular resolution is demonstrated. By means of implementation of a hollow optical fiber as the sample cuvette, the observation of living cells in different 3-D matrices is enabled. The fiber delivers a stable and accurate rotation of a cell or cell cluster, providing quantitative phase data for tomographic reconstruction of the 3-D refractive index distribution with an isotropic spatial resolution. We demonstrate that it is possible to clearly distinguish and quantitatively analyze several cells grouped in a "3-D cluster" as well as subcellular organelles like the nucleoli and local internal refractive index changes. © 2014 Society of Photo-Optical Instrumentation Engineers (SPIE) [DOI: 10.1117/1.JBO.19.4.046009]

1 Introduction

Recent research has proved that for anticancer drug response testing it is more advisable to use three-dimensional (3-D) rather than two-dimensional cell models. So far, it has been demonstrated that cells cultured in 3-D behave differently and reflect cancer cells in their real environment in a better way.[1] Processes in 3-D cell models have already been widely addressed with molecular specificity by fluorescence microscopy.[2] However, in many cases, the sample has to be modified by antibodies, dyes, genetic transfection, or exposed to a high light intensity. Thus, novel, minimally invasive 3-D imaging techniques, which affect the sample as little as possible, are of high interest. Our research falls in line with these current trends as recently digital holography has provided the numerical access to the complex optical field and digital holographic microscopy (DHM) has found numerous applications in the quantitative investigation of biological micro-objects.[3–7] Specifically, investigation of cells in transmission with quantitative DHM phase contrast method gained a lot of interest.[8,9] However, data captured from a single direction of observation yields the integrated phase information about optical path changes[10,11] and despite its capabilities to reconstruct images of objects at different distances, DHM cannot provide 3-D distribution of the refractive index. In order to overcome this limitation, the integrated phase data, acquired by digital holography from many directions, should be combined with tomographic reconstruction concepts.[12–20] Alternatively, instead of using DHM, this might be achieved with related methods such as diffraction phase microscopy[21] or currently developed spatial light interference tomography,[22,23] which now evolved into white-light diffraction tomography.[24] Nevertheless, several authors have already implemented tomographic procedures based on holography for 3-D refractive index investigations inside cells. The projections of

an object are captured based on two different approaches: (1) altering the illumination angle[12–16] or (2) rotation of a bio-sample introduced into a fiber capillary[18,19,25] or alternatively subjected to rotation by optical tweezers.[26] In the first approach, the data about an object are provided by projections captured within a limited angle and therefore, more complicated and less accurate tomographic algorithms are applied for object reconstruction.[27–29] In the second approach, in most cases, projections from a full angle are available, which simplifies the tomographic analysis. However, the application of optical tweezers significantly complicates the measurement system.[26] Also, the energy required for creating optical tweezers may influence or even damage the investigated cells,[30,31] especially at longer measurement times, which are required to acquire all the projections. The concept of inserting cells into a rotatable capillary has been proven to be a functional solution in many studies.[18,19,25] Thus, in this paper, we focus on both hardware and numerical enhancements of this concept. We have also decided to combine this solution with capturing phase data in a self-interference digital holographic microscope (SIDHM),[9] which differentiates this implementation from the work of other groups.[18,19,25] The SIDHM configuration guarantees low sensitivity to vibration and environment instabilities and therefore is well suited to measure the numerous (most often 90 or more) phase projections of an investigated cell. In Sec. 2, we describe the main modules of the tomographic phase microscope (TPM) and the data processing scheme. In Sec. 3, we demonstrate the functionality of our system through providing the results of measurements—cancer cells with different morphological features and present tomographic phase imaging of a 3-D cell culture with subcellular resolution. We also describe an optional calibration procedure for absolute refractive index measurement by using internalized microspheres.

---

*Address all correspondence to: Arkadiusz Kuś, E-mail: a.kus@mchtr.pw.edu.pl

2 Measurement Setup for TPM

The utilized TPM, based on digital holography, is composed of several modules including self-interference DHM, rotary fiber holder, and data capture and processing unit. In the following sections, we describe these modules.

2.1 Self-Interference Digital Holographic Microscope

The phase projections are captured by an SIDHM.[9] In comparison to a common transmission DHM based on Mach–Zehnder interferometer configuration,[32] the SIDHM is highly insensitive to vibration due to replacing a reference beam with a shearing module realized by a Michelson interferometer (Fig. 1). In the setup, two sheared object wavefronts are superimposed.

In the self-interference configuration, used for phase tomography, the sample is illuminated in transmission with coherent light from a frequency doubled Nd:YAG laser ($\lambda = 532$ nm) via a single mode optical fiber and the microscope condenser (CL). Optical imaging of the sample is performed by a Zeiss achromatic microscope objective [Zeiss LD Achroplan 20×0.4 Corr. numerical aperture (NA) 0.4)] with a long working distance (10 mm) and the nontilted mirror (M1) of the Michelson interferometer. The second mirror (M2) is tilted in such a way that an area without a sample is superimposed with the wavefront that is transmitted through the sample. Thus, a reference wave is generated that is not disturbed by the sample. The digital holograms are captured by a charge coupled device (CCD) sensor (Basler pia-2400-12gm camera, pixel size: 3.45 μm) and then evaluated numerically aiming for accurate determination of an object phase ϕ_o at a plane conjugate with an object. The first step of this procedure was to calculate the phase in the hologram plane ϕ_h. This
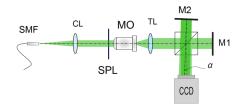

Fig. 1 Self-interference DHM: SMF, single mode fiber; CL, condenser lens; SPL, specimen plane; MO, microscope objective; TL, tube lens, M1 and M2, mirrors, α, M2 tilt angle; and CCD, CCD camera.

was performed by spatial phase shifting as described in Refs. 33 and 34. The proper operation of SIDHM for phase retrieval in combination with approaches in Refs. 33 and 34 has already been demonstrated and verified in Ref. 35 and in the supplementary information of Ref. 36 by data from silica and polystyrene microspheres. The imaging system provided the overall Abbe resolution $\lambda/2$NA of 0.67 μm and spatial sampling of the object equal to 0.18 μm. The further steps of hologram processing for tomographic phase imaging are described in Sec. 2.3.

2.2 Rotary Fiber Holder

Tomography requires capturing numerous digital holograms of an object from different directions. To fulfill this requirement, we had proposed at first to implement a hollow optical fiber as a cuvette for a cell or a cell group and subsequently place the fiber in an accurate rotary fiber holder. It should be emphasized that such solution requires only a minor modification of SIDHM prior to 3-D cell measurement and it does not involve additional optical components. The idea behind the mechanical rotation of a fiber capillary is to provide a tool capable of cell cultivation as well as measurement of 3-D biological structures. The main feature of this concept is the fact that cells—once placed in a hollow fiber—grow in a similar way as in a Petri dish. This concept is comparable to using a micropipette in order to rotate the sample,[19] although in our case, there is no mechanical intrusion in the specimen. Moreover, by virtue of the capillary attraction, it is not necessary to use plugs to prevent cell culture medium from flowing out. However, in order to avoid strong diffraction and refraction phenomena due to the cylindrical shape of the capillary and also to allow high accuracy holographic measurements, it is necessary to insert the fiber cuvette into an immersion liquid[32] as shown in Fig. 2(a). A standard microscope stage has been replaced with a custom-designed one, which consists of a Petri dish support and an Elliot Martock rotary fiber holder. The holder, which offers an angular resolution of <0.01 deg, assured high precision of the specimen position for each acquired projection. A cell, once inserted in the hollow fiber, can be properly placed in the field of view through 3-D manipulation of the fiber. The fiber capillary (inner diameter: 212 μm, outer diameter: 300 μm) has been made of Hereaus fused silica with refractive index of $n = 1.46071$ at $\lambda = 532$ nm. The inner surface of the fiber was treated with 0.5% polyvinyl alcohol in order to prevent
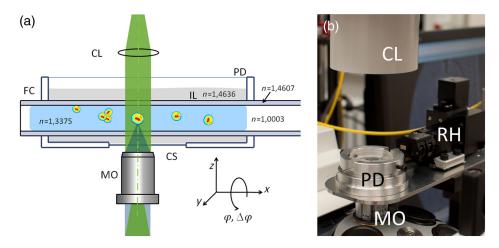

Fig. 2 The rotary fiber holder setup: (a) scheme and (b) photo. CL, condenser lens; PD, Petri dish; IL, immersion liquid; FC, fiber capillary; MO, microscope objective; (x, y, z, ϕ), movement directions of the fiber capillary; $\Delta\phi$, rotation step for N projections; RH, rotary holder; and CS, cover slip.

cells from attaching to the fiber walls.[37] The fiber was placed inside a modified Petri dish (μ-Dish, ibidi GmbH, Munich, Germany), filled with immersion liquid (refractive index $n = 1.4636$ at $\lambda = 532$ nm) matched to the capillary material.

The bottom of the used Petri dish (PD) is a 0.17 mm cover slip. Since the microscope objective has been designed to work with such CSs, this ensures proper working conditions for the imaging system. The use of the immersion liquid reduced the cylindrical lens effect caused by the shape of the hollow fiber. The remaining lens effect caused by the difference between cell culture medium and fiber refractive indices was removed numerically.[38]

2.3 Tomographic Reconstruction

The flow chart of the applied procedures for phase tomography is presented in Fig. 3. In order to obtain a successful 3-D reconstruction of an object, it is necessary to acquire a set of phase images corresponding to a series of angular projections of an object. In this work, 180 projections were captured with the angle of rotation between sequential measurements equal to 1 deg. For each projection, captured with SIDHM within a specified area of interest [see Fig. 3(a)], the integrated phase ϕ_h in the hologram plane has been calculated.[33,34] Then, all phases were propagated using a convolution approach to obtain phase ϕ_o in the object plane. This approach takes into consideration the diffraction effects and therefore allows for the application of the filtered backprojection[39] method for tomographic reconstruction in case of phase objects.[40] In order to find the object plane (the plane of best focus) for each projection, the numerical autofocusing algorithm was applied.[41] The complex object wave was numerically propagated to the successive planes and then the real amplitude was reconstructed in order to evaluate the focus. Cells in a 3-D collagen matrix are treated as phase-only objects, thus the criterion for the best focused image was based on the lowest detail in the amplitude distribution. The holograms were assessed automatically using the method based on calculating the variance of optical field modulus, as proposed in Ref. 41. Next, the influence of the fiber capillary on the phase distribution has been corrected by means of subtraction of an estimated aberration profile, which was created using areas of a hologram not containing any cells.[38,42] What is

more, radial cell position run-out correction has been performed in the specimen plane. The position of a cell under study has been tracked using a phase value threshold and the calculation of the first moment of the area of a cell in the field of view, as described in Ref. 43. Then, the phase images were cropped in order to keep the center of the investigated cell or cell cluster in the middle and thus minimize reconstruction artifacts.[44] The resulting phase distributions ϕ_{o_corr}, having undergone the aberration removal and radial run-out correction [Fig. 3(b)], were additionally filtered with a small median filter (3×3 pixels) and were then used as an input for phase tomography algorithm. The 180 phase projections (acquired at an angular step $\Delta\alpha = 1$ deg) were then used to create sinograms [Fig. 3(c)], and later reconstructed in the second step by means of the Filtered Backprojection method as reported in Refs. 39, 40, 45, and 46. This approach requires the assumption that the object under study introduces only slow-varying phase changes in the object wave. This condition is expected to be fulfilled by the small differences between the cells and the surrounding collagen matrix refractive indices. Furthermore, the object phase is propagated to the center of the object. Thus, the diffraction effects caused by the object are minimized and therefore assumed to be neglectable.

The full 3-D distribution of phase values was achieved by sequentially assembling the cross sections of the reconstructed phase differences $\Delta\Phi(x, y, z_0 \div Z)$. Then, the results for each reconstructed layer z_i have been scaled to the refractive index difference values Δn (relative values of refractive index) according to

$$\Delta n(x, y, z_i) = \frac{\Delta\Phi(x, y, z_i)\lambda}{2\pi d}, \qquad (1)$$

where $\Delta\Phi(x, y, z_i)$ is the phase difference calculated for the layer z_i, d represents the thickness of the layer z_i, which depends on the dimension of CCDs pixel calculated in the object plane and λ is the wavelength of the light source used to obtain the phase images [Fig. 3(d)].

The determination of the absolute cellular refractive index value n requires the knowledge of the exact value of the refractive index of the medium that surrounds the cells, which plays a role of an immersion liquid n_{ref} and thus serves as a reference medium:
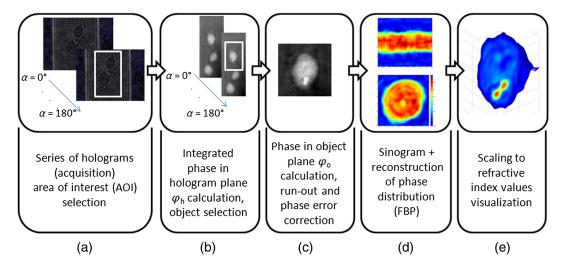

Fig. 3 The flowchart of the procedures for the reconstruction and visualization of the three-dimensional (3-D) refractive index distributions.

$$n(x, y, z_i) = \frac{\Delta\Phi(x, y, z_i)\lambda}{2\pi d} + n_{\mathrm{ref}}. \tag{2}$$

The uncertainties of the refractive index can be quantified using the exact differential method:

$$u_n = \partial\Phi\frac{\lambda}{2\pi d} + \partial\lambda\frac{\Phi}{2\pi d} + \partial d\frac{\Phi\lambda}{2\pi d^2} + u_{\mathrm{n\_ref}} = u_{\mathrm{n\_r}} + u_{\mathrm{n\_s}}. \tag{3}$$

The first summand of Eq. (3) is the random error $u_{\mathrm{n\_r}}$ ($[\partial\Phi(\lambda/2\pi d)]$) of the measurement. The next three summands consider the systematic error $u_{\mathrm{n\_s}}$. The systematic error $u_{\mathrm{n\_s}}$ includes the contributions of the errors that originate from the uncertainties of the devices (spectral width of the laser source, pixel size of the camera, etc.) used in the experimental setup ($\partial\lambda(\Phi/2\pi d) + \partial d(\Phi\lambda/2\pi d^2) = 0.0037$), which are constant for every measurement and the uncertainty $u_{\mathrm{n\_ref}}$ of the refractive index n_{ref} of the collagen that surrounds the cells. Unfortunately, the density of the collagen matrix inside the optical fiber is spatially inhomogeneous and depends on the preparation procedure. Thus, the refractive index uncertainty of the collagen matrix can be estimated to be high ($u_{\mathrm{n\_ref}} \approx 0.01$). The random error resulting from the phase measurements and the filtering procedure is estimated as $u_{\mathrm{n\_r}} = 0.0005$. In summary, the uncertainty of the absolute refractive index values is high ($u_n = 0.0142$) and strongly depends on the uncertainty of the refractive index of the reference medium. For this reason, the results in Figs. 4–6 are presented in relative refractive index values, for which the uncertainty is much lower ($u_n = 0.0042$). However, the scaling process could be enhanced if the refractive index markers in the form of microspheres with a known refractive index[35] were introduced into the measurement volume. This approach is reported in Sec. 3.2.

The processing of all the measurement data necessary to reconstruct the tomographic phase images was performed by custom-built MATLAB scripts. In order to improve the data visualization, surface representations were created with a threshold-based filtering of the refractive index values that correspond to the refractive index levels of background of the observed cells.
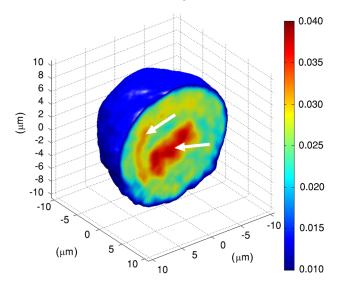

Fig. 5 The relative refractive index distribution inside an HT-1080 cell group at several cross sections (of the same cell cluster). Refractive index peak to valley value $\Delta n = 0.030 \pm 0.004$ (Video 2, MPEG, 4.6 MB) [URL: http://dx.doi.org/10.1117/1.JBO.19.4.046009.2].

3 Results and Discussion

The experiments have been focused on investigations of cancer cells and cancer cell clusters with different geometrical and internal refractive index distribution features. The main goal of the measurements was proving the capabilities of the developed tomographic system to accurately reconstruct the 3-D refractive index distributions inside cells and cell clusters.

3.1 Biological Samples

The chosen biological samples were human malignant lymphoma cells (U937) and human fibrosarcoma cells (HT-1080). Both cell types were cultivated in Dulbecco's modified Eagle's medium (Biochrom AG, Berlin) supplemented with 10% fetal calf serum (Biochrom AG, Berlin) at 37°C and 10% CO_2 atmosphere. Some of HT-1080 cells were additionally incubated for one night with uncoated silica (SiO_2) microspheres (Mikropartikel, GmbH, Berlin, Germany) in order to enable incorporation of the

Fig. 4 The relative refractive index distribution inside a single U937 cell. Refractive index peak to valley value $\Delta n = 0.030 \pm 0.004$ (Video 1, MPEG, 2.2 MB) [URL: http://dx.doi.org/10.1117/1.JBO.19.4.046009.1].
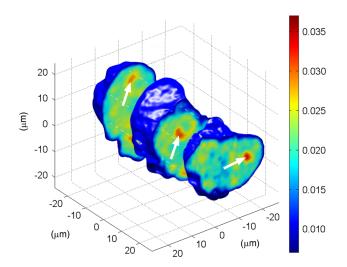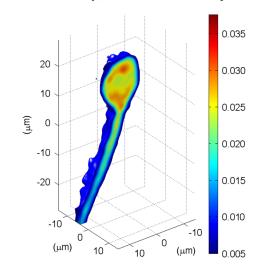

Fig. 6 The relative refractive index distribution in an HT-1080 cell with an extension, vertical cross sections through the cell. Refractive index peak to valley value $\Delta n = 0.032 \pm 0.004$ (Video 3, MPEG, 2.2 MB) [URL: http://dx.doi.org/10.1117/1.JBO.19.4.046009.3].

particles into the cells by phagocytosis.[35] These particular cells were applied to illustrate the procedure of determination of the absolute refractive index values inside a cell. Then, the cells were detached and suspensions of 10^6 cells/ml were prepared. To inert the U937 cells, the suspension was mixed with an agar solution to a final concentration of 0.15% agar. The suspended HT-1080 cells were mixed with collagen to a final concentration of 0.16% collagen. The prepared agar and collagen mixtures were introduced into the hollow fibers by capillary attraction. Such mixture, especially the cultivation in collagen, helped to avoid cell tumbling during the rotation in the measurement process. Owing to the viscosity of the medium and the small moment of inertia of cells, there is no visible movement of cells due to the measurement procedures. However, this matter should be separately investigated in the future. Lymphoma cells were observed directly after the preparation. Fibrosarcoma cells were cultured for additional 24 h to allow polymerization of the collagen fibers and permit cells to migrate inside the matrix. HEPES buffer has been added to the collagen cell mixture to compensate for the missing CO_2 atmosphere.[35] All tomographic measurements were performed at a room temperature ($T = 22°C$) in order to prevent the fast cell migrations during our proof of principle experiments.[35,36] Although this is not the perfect incubation temperature for cells, the specimens were not influenced significantly by this fact, as the measurement was performed within no more than 2 h after the environment had changed. The cells with a typical appearance were selected for the measurements. There was no need for an additional heating chamber in the setup. However, the device is suitable to be integrated into an incubation system for extended time-lapse investigations in the future.

3.2 Experimental Results

The cells described in Sec. 3.1 were used as the specimens measured in the TPM. For each measurement object, 180 images were acquired at the rate of 1 Hz. At first, a single U937 cell with spherical appearance, which was randomly chosen from the cell distribution in the fiber capillary, was measured. It is the least complex measurement object of the whole measurement series presented in this paper. The reconstructed relative refractive index distribution in this cell is shown in Fig. 4. The nuclear envelope and density changes in the nucleus (see arrows in Fig. 4) are clearly visible.

Next, the capability to measure the clusters of cells is demonstrated. The refractive index distribution in a cluster of five HT-1080 cells in collagen with several individual cross sections through the cells is presented in Fig. 5. Here, nucleoli are visible inside the cells, which greatly help to distinguish between the cells and to count them (see arrows in Fig. 5 and Video 2). Owing to the subcellular resolution, it is possible to observe cell walls and to assess the interaction between the cells. This result appears to be of particular importance when cell clusters in 3-D cell matrices are treated with drugs.

Employing our method shows up prospects to compare such a cell cluster before and after the treatment with drugs or toxins in order to trace internal changes in cell structure within a cell group. Furthermore, we applied our tomographic system to measure a highly nonsymmetrical object, namely to study HT-1080 cells with the developed extensions. The result is shown in Fig. 6.

The results presented in Figs. 4–6 are given in the values of a relative refractive index Δn. However, it is also of interest to rescale the data to absolute refractive index values as these values are directly related to the intracellular solute concentrations and the dry mass.[47,48] As it has already described in Sec. 2.3, it is not suitable to use the refractive index of the surrounding medium as a reference in our study. However, the refractive index values can be obtained if an object with a well-known refractive index value, such as silica microspheres that are internalized by living cells, is present in the measurement volume. Such a case is presented in Fig. 7, where two silica beads are clearly resolved inside an HT-1080 cell [see label "1" in Fig. 7(a)]. As the refractive index of uncoated silica microspheres was measured to be equal to $n_{ref} = 1.435 \pm 0.003$,[35] it is possible to calibrate the measurement of the cell to obtain the absolute refractive index values with total uncertainty (see Sec. 2.3) equal to 0.0072. Rescaling the former relative refractive index variations to the absolute refractive index values
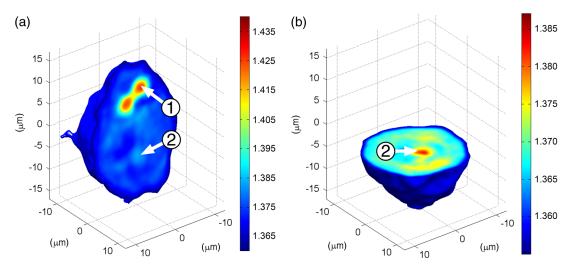

Fig. 7 The 3-D refractive index distribution of an HT-1080 cell with incorporated SiO_2 microspheres with refractive index $n = 1.435 \pm 0.003$ and diameter $\emptyset \approx 3.44$ μm; (a) vertical cross section through the absolute refractive index (peak to valley value $\Delta n = 0.080 \pm 0.007$) (Video 4, MPEG, 2.2 MB) [URL: http://dx .doi.org/10.1117/1.JBO.19.4.046009.4] and (b) horizontal cross section through the same cell, absolute refractive index values. Here, image scale is adjusted to the refractive index of a nucleolus (refractive index peak to valley value $\Delta n = 0.030 \pm 0.007$).

provides the full quantitative measurement data. The refractive index value of a nucleolus of the cell is obtained as $n = 1.385 \pm 0.0072$ and represents the highest refractive index inside the cell—apart from the silica microspheres (see label "2," Fig. 7). The detected refractive index changes inside the cell (Fig. 7) were found in agreement with the previously published data.[20,35] However, it should be noted that introducing an object with a step refractive index into a cell is a source of a locally strong phase gradient, while the main assumption that allowed for using the FBP algorithm was that only weak spatial variations of phase should be present. This leads to a conclusion that, besides causing possible changes of the intracellular structure, an inappropriate calibration object may cause additional significant errors in the reconstructed refractive index distribution. Nevertheless, in our case, we were able to avoid the impact of diffraction on the FBP algorithm as a result of the propagation applied as described in Sec. 2.3. In fact, the image artifacts were sufficiently small to successfully retrieve the absolute refractive index distribution of a living cell.

4 Conclusion

In this paper, we have presented a successful development and application of the SIDHM in combination with a sample-rotation-based tomography module for 3-D label-free quantitative live cell imaging with subcellular resolution. When compared to the systems consisting of acousto-optic modulators[20] or a spatial light modulator,[23] the most expensive component, required to modify the holographic microscope for tomography, is in our case the rotary fiber holder. However, when mechanical rotation of a sample is used as the only means of acquiring tomographic projections, the overall measurement time limits the possibility to measure the dynamic processes. The resolution of the system is restricted by the NA of the imaging system. The possibility to overcome this limitation is to use tomography with altering the illumination direction.[27–29] In this case, at the expense of anisotropic spatial frequency coverage, the maximum resolution can be at least doubled.[49–51] The additional application of complex deconvolution methods prospects even a further resolution enhancement down to the nanometer scale.[14] Our results prove the suitability of the method to study both quasisymmetrical and highly nonsymmetrical objects of a complex internal structure for objects with small internal variations of the refractive index. We have demonstrated that it is possible to clearly distinguish several cells in a "3-D cluster" and subcellular organelles in cells. The detected structures correspond well to the results from the earlier live cell investigations with a quantitative phase contrast,[52] a comparative study with a DHM and the fluorescence microscopy on the nucleus components[53] and the results from the TPM.[35,54] Thus, they can be identified as nucleoli, the nuclear envelope and chromatin density changes. By means of implementation of a hollow optical fiber as the cuvette for the sample, observation of living cells in different 3-D matrices is enabled. The fiber mounted in the rotary holder delivers stable and accurate rotation of a cell or cell cluster, providing quantitative phase data for tomographic reconstruction of 3-D refractive index distributions with isotropic spatial resolution. However, due to the cylindrical shape of the sample cuvette, it must be located in an immersion liquid and the eventual residual phase error introduced by the fiber capillary has to be removed numerically. We also propose a methodology for absolute refractive index determination by means of calibrating the values using a reference object with well-known properties.

In order to minimize the uncertainty of absolute refractive index values, it is advisable to measure the refractive index of an applied calibration marker with the best possible accuracy.

The concept of rotating the specimen is especially convenient when a condenser and objective lens with a long working distance are utilized. Using a conventional biological microscope setup for tomographic DHM measurements is a step toward applying standard microscopy equipment such as regular heating chambers in tomography to incubate specimen in the capillary. Although it is possible to measure the refractive index values, it would be also beneficial to obtain other 3-D information, e.g., the volume and the area of the selected substructures. The procedures of applying a threshold for refractive index in the measurement data in order to extract interesting features are under development. In the future, the methodology and equipment presented in this paper will be further adapted with the aim to study various cell infection and treatment scenarios.

References

1. C. Fischbach et al., "Engineering tumors with 3D scaffolds," *Nat. Methods* **4**(10), 855–860 (2007).
2. C. C. Park et al., "Rapid and automated multidimensional fluorescence microscopy profiling of 3D human breast cultures," *Integr. Biol.* **5**(4), 681–691 (2013).
3. M. K. Kim, in *Digital Holographic Microscopy: Principles, Techniques and Applications*, Springer, New York (2011).
4. E. Cuche, P. Marquet, and C. Depeursinge, "Simultaneous amplitude contrast and quantitative phase contrast microscopy by numerical reconstruction of Fresnel off-axis holograms," *Appl. Opt.* **38**(34), 6994–7001 (1999).
5. B. Kemper and G. von Bally, "Digital holographic microscopy for live cell applications and technical inspection," *Appl. Opt.* **47**(4), A52–A61 (2008).
6. B. Kemper, P. Langehanenberg, and A. Bauwens, "Digital holographic microscopy techniques for multi-focus quantitative phase imaging of living cells," in *Biomedical Optical Phase Microscopy and Nanoscopy*, N. Shaked, Z. Zalevsky, and L. L. Satterwhite, Eds., pp. 97–129, Academic Press, Waltham, Massachusetts (2012).
7. K. Lee et al., "Quantitative phase imaging techniques for the study of cell pathophysiology: from principles to applications," *Sensors* **13**(4), 4170–4191 (2013).
8. C. J. Mann et al., "High resolution quantitative phase contrast microscopy by digital holography," *Opt. Express* **13**, 8693–8698 (2005).
9. B. Kemper et al., "Simplified approach for quantitative digital holographic phase contrast imaging of living cells," *J. Biomed. Opt.* **16**(2), 026014 (2011).
10. B. Rappaz et al., "Measurement of the integral refractive index and dynamic cell morphometry of living cells with digital holographic microscopy," *Opt. Express* **13**(23), 9361–9373 (2005).
11. B. Kemper et al., "Integral refractive index determination of living suspension cells by multifocus digital holographic phase contrast microscopy," *J. Biomed. Opt.* **12**(5), 054009 (2007).
12. M. Debailleul et al., "High-resolution three-dimensional tomographic diffractive microscopy of transparent inorganic and biological samples," *Opt. Lett.* **34**(1), 79–81 (2009).

13. R. Fiolka et al., "Simplified approach to diffraction tomography in optical microscopy," *Opt. Express* **17**(15), 12407–12417 (2009).
14. Y. Cotte et al., "Marker-free phase nanoscopy," *Nat. Photonics* **7**, 113–117 (2013).
15. B. Simon et al., "High resolution tomographic diffractive microscopy of biological samples," *J. Biophotonics* **3**(7), 462–467 (2010).
16. Y. Sung et al., "Optical diffraction tomography for high resolution live cell imaging," *Opt. Exp.* **17**(1), 266–277 (2009).
17. A. Barty et al., "Quantitative phase tomography," *Opt. Commun.* **175**(4–6), 329–336 (2000).
18. F. Charrière et al., "Cell refractive index tomography by digital holographic microscopy," *Opt. Lett.* **31**(2), 178–180 (2006).
19. F. Charrière et al., "Living specimen tomography by digital holographic microscopy: morphometry of testate amoeba," *Opt. Express* **14**(16), 7005–7013 (2006).
20. W. Choi et al., "Tomographic phase microscopy," *Nat. Methods* **4**, 717–719 (2007).
21. G. Popescu et al., "Diffraction phase microscopy for quantifying cell structure and dynamics," *Opt. Lett.* **31**(6), 775–777 (2006).
22. Z. Wang et al., Spatial light interference tomography (SLIT), *Opt. Exp.* **19**(21), 19907 (2011).
23. M. Mir et al., Visualizing Escherichia coli sub-cellular structure using sparse deconvolution spatial light interference tomography, *PLoS One* **7**(6), e38916 (2012).
24. T. Kim et al., "White-light diffraction tomography of unlabelled live cells," *Nat. Photonics* **8**, 256–263 (2014).
25. M. Fauver et al., "Three-dimensional imaging of single isolated cell nuclei using optical projection tomography," *Opt. Exp.* **13**(11), 4210–4223 (2005).
26. M. K. Kreysing et al., "The optical cell rotator," *Opt. Exp.* **16**(21), 16984–16992 (2008).
27. D. Verhoeven, "Limited-data computed tomography algorithms for the physical sciences," *Appl. Opt.* **32**(20), 3736–3754 (1993).
28. A. Likhachov, "Projection data replenishment algorithm for limited angle tomography," *Optoelectron. Instrum. Data Process.* **45**(1), 55–61 (2009).
29. K. C. Tam and V. Perez-Mendez, "Tomographical imaging with limited-angle input," *J. Opt. Soc. Am.* **71**(5), 582–592 (1981).
30. H. Zhang and K. Liu, "Optical tweezers for single cells," *J. R. Soc. Interface* **5**(24), 671–690 (2008).
31. D. Carl et al., "Parameter-optimized digital holographic microscope for high-resolution living-cell analysis," *Appl. Opt.* **43**(36), 6536–6544 (2004).
32. P. Kniażewski, T. Kozacki, and M. Kujawińska, "Inspection of axial stress and refractive index distribution in polarization-maintaining fiber with tomographic methods," *Opt. Lasers Eng.* **47**(2), 259–263 (2009).
33. K. C. Neuman, "Characterization of photodamage induced by optical tweezers," paper presented at the *Conference on Technical Digest, Lasers and Electro-Optics, 1998 (CLEO 98)*, pp. 203–204, IEEE, San Francisco, California (1998).
34. B. Kemper et al., "Investigation of living pancreas tumor cells by digital holographic microscopy," *J. Biomed. Opt.* **11**(3), 034005 (2006).
35. S. Przibilla et al., "Sensing dynamic cytoplasm refractive index changes of adherent cells with quantitative phase microscopy using incorporated microspheres as optical probes," *J. Biomed. Opt.* **17**(9), 097001 (2012).
36. A. Barroso et al., "Three-dimensional exploration and mechano-biophysical analysis of the inner structure of living cells," *Small* **9**(6), 885–893 (2013).
37. K. Ziółkowska et al., "Long-term three-dimensional cell culture and anticancer drug activity evaluation in a microfluidic chip," *Biosens. Bioelectron.* **40**(1), 68–74 (2013).
38. J. Kostencka et al., "Holographic method for capillary induced aberration compensation for 3D tomographic measurements of living cells," *Proc. SPIE* **8792**, 879204 (2013).
39. F. Natterer, *The Mathematics of Computerized Tomography*, Wiley, New York (1986).
40. T. Kozacki, M. Kujawińska, and P. Kniazewski, "Investigating the limitation of optical scalar field tomography," *Opto-Electron. Rev.* **15**, 102–109 (2007).
41. J. Kostencka, T. Kozacki, and K. Liżewski, "Autofocusing method for tilted image plane detection in digital holographic microscopy," *Opt. Commun.* **297**, 20–26 (2013).
42. T. Kozacki, R. Krajewski, and M. Kujawińska, "Reconstruction of refractive-index distribution in off-axis digital holography optical diffraction tomographic system," *Opt. Express* **17**(16), 13758–13767 (2009).
43. R. C. Gonzales and R. E. Woods, *Digital Image Processing*, 3rd ed., Prentice Hall Inc., Upper Saddle River, New Jersey (2007).
44. Y. Jeon and C. K. Hong, "Rotation error correction by numerical focus adjustment in tomographic phase microscopy," *Opt. Eng.* **48**(10), 105801 (2009).
45. W. Górski and M. Kujawinska, "Three-dimensional reconstruction of refractive index inhomogeneities in optical phase elements," *Opt. Lasers Eng.* **38**(6), 373–385 (2002).
46. M. Kujawinska et al., "Interferometric and tomographic investigations of polymer microtips fabricated at the extremity of optical fibers," *Proc. SPIE* **8494**, 849404 (2012).
47. G. Popescu et al., "Optical imaging of cell mass and growth dynamics," *Am. J. Physiol. Cell Physiol.* **295**(2), C538–C544 (2008).
48. B. Rappaz et al., "Noninvasive characterization of the fission yeast cell cycle by monitoring dry mass with digital holographic microscopy," *J. Biomed. Opt.* **14**(3), 034049 (2009).
49. S. Vertu et al., "Diffraction microtomography with sample rotation: influence of a missing apple core in the recorded frequency space," *Cent. Eur. J. Phys.* **7**, 22–31 (2009).
50. S. Vertu et al., "Comparison of resolution in tomographic diffractive microscopy using combinations of sample rotation and illumination rotation," *Proc. SPIE* **7904**, 79041O (2011).
51. C. J. R. Sheppard and S. S. Kou, "3D imaging with holographic tomography," in *AIP Conf. Proc.*, Vol. 1236, pp. 65–69 (2010).
52. B. Kemper et al., "Label-free quantitative cell division monitoring of endothelial cells by digital holographic microscopy," *J. Biomed. Opt.* **15**(3), 036009 (2010).
53. B. Kemper et al., "Influence of sample preparation and identification of subcellular structures in quantitative holographic phase contrast microscopy," *Proc. SPIE* **7715**, 771504 (2010).
54. C. Fang-Yen et al., "Video-rate tomographic phase microscopy," *J. Biomed. Opt.* **16**(1), 011005 (2011).

Arkadiusz Kuś is a PhD student at Warsaw University of Technology. He received his MSc Eng degree in automation and robotics with specialization in photonics engineering from Warsaw University of Technology, Faculty of Mechatronics in 2011. Apart from his scientific career, he also worked for the company PZO microscopes and optical devices, LTD, located in Warsaw, Poland. His current research interests include optical diffraction tomography, holography, and optical design.

Michal Dudek graduated in applied physics (specialization—photonics) from Faculty of Physics, Warsaw University of Technology in 2011. Since 2011, he has been a PhD student at the Institute of Micromechanics and Photonics, Warsaw University of Technology. He is participating in the three-dimensional phase project within the TEAM program and his main field of interest is tomographic (interferometric and holographic) analysis of technical and biological microstructures. He is a member of SPIE.

Björn Kemper is a senior researcher at the Biomedical Technology Center of the Medical Faculty, University of Münster, Germany. He received his PhD in physics from the Humboldt Universität zu Berlin, Germany, in 2001. His research interests are optical metrology and biomedical optics with main focus on optical microscopy. He is author and co-author of more than 100 publications in peer reviewed journals, book chapters, and conference proceedings.

Malgorzata Kujawińska is a full professor of applied optics at Warsaw University of Technology and she is a head of the Photonics Engineering Division at Institute of Micromechanics and Photonics. She has been involved in the optical metrology topics since 1980's including development of interferometric, holographic, grating interferometry, diffraction tomography, digital image correlation, and structured light-based methods. She has authored one monograph, several book chapters, and more than 200 papers in international scientific journals. She is a fellow of SPIE.

Biography of Angelika Vollmer is not available.